Optimization of assembly accuracy control in aircraft manufacturing and accuracy improvement strategies by finite element analysis methods

Abstract: The parallel mechanism has the advantages of good posturing performance, fast response, high precision and strong load carrying capacity, and its application in flexible positioning of machine assembly has shown significant technical advantages in recent years. This paper proposes a 3-UPS parallel configuration based on the aircraft assembly posturing and positioning mechanism, which can realize the 6-degree-of-freedom posturing and positioning of the aircraft component assembly. At the same time, in order to improve the precision of vehicle assembly, the influence of the error gap between the hinges of each motion vice on the attitude of the vehicle assembly attitude adjustment and positioning mechanism is analyzed, and the effective rod length model of the 3-UPS parallel connection mechanism is established accordingly. Further, based on the assembly level, order and constraint information, the assembly deviation transfer model of the 3-UPS attitude positioning mechanism was obtained. Finally, the optimization effect of calibration and compensation of geometric error is analyzed by finite element. The results show that the maximum position error of the vehicle assembly is reduced from 0.371mm to 0.037mm after optimization and compensation, and the motion accuracy of the mechanism is improved by one order of magnitude compared with that before compensation. The maximum attitude error is reduced from the original 1.18×10^{-2} rad to 5.940×10^{-4}. It is verified that the method of this paper is effective for reducing the positional error of the moving platform of the parallel mechanism and improving the assembly accuracy of the vehicle assembly.

Keywords: Aircraft assembly, parallel mechanism, deviation transfer, attitude adjustment and positioning mechanism; finite element analysis.

1. Introduction

The aircraft assembly process is a complex process, compared with general

mechanical products, its assembly process contains a large number of parts, components, fixtures and equipment and other manufacturing resources, with complex coordination relationships, huge workloads and long assembly cycle and other characteristics, especially for the assembly quality requirements are extremely strict [1-3]. Vehicle assembly process as the basic unit of assembly, process quality control is the key to ensure the quality of vehicle assembly process and final product quality [4-5]. Vehicle assembly processes are divided into critical processes and non-critical processes. Among them, critical assembly processes refer to the assembly processes that have a direct impact on the final product quality and the processes that generate more problems in the assembly process [6-8]. If the quality of critical assembly processes at the assembly site cannot be controlled, it is difficult to ensure the stability of assembly quality [9]. In addition, the assembly accuracy of vehicle components largely determines the assembly quality of the vehicle [10-11]. At present, product accuracy is mainly ensured by analyzing and controlling the assembly accuracy in the preparation stage of the assembly process [12-13]. Therefore, to address the quality problem of excessive assembly accuracy due to the accumulation of actual errors of components during the actual assembly of aircraft on site, the quality control technology of key assembly processes of aircraft based on the analysis of assembly accuracy is proposed [14-16]. By preprocessing the measured data and establishing an assembly process accuracy model based on measured data, the assembly accuracy analysis of key assembly processes in the field is realized.

Complex precision mechanical products in the actual assembly process, from time to time, due to the unreasonable precision design leads to low assembly accuracy, poor assemblability, and even rework and other problems, a large number of assembly accuracy control optimization methods into the vision of experts and scholars.Guo, F. et al. through the key features optimization method and assembly station flow fluctuation analysis method to control the quality of the equipment of the flying machine, according to the feedback results of the equipment control action Plotting the trajectory of assembly error and fluctuation, which can dynamically understand the change of assembly quality and help the stable and rapid production of flying

vehicles [17]. Wang, Q. et al. established a gap tolerance constraint constraint model in the assembly process of a vehicle, derived the relational equation of the assembly part gap with attitude change by auxiliary positioning point estimation and small attitude transformation method, and solved it by using optimization optimization seeking method to minimize the overall gap and control the excess gap within the tolerance [18]. Guo, F. et al. showed that the propagation of manufacturing errors in aircraft products is unavoidable during the assembly process, and in response to this problem, a coordinated dimensional chain of different assemblies is established and the final error is coordinated by controlling and optimizing the direction and value of the cumulative error range [19]. Yu, L. et al. designed a non-contact measurement method of normal vectors and heights of mesosurfaces based on laser displacement sensors and a specialized CNC machine for normal vector adjustment to determine the real position of the workpiece at the drilling position and its 3D geometry during the assembly process of the vehicle [20]. Guo, F. et al. proposed an error compensation method based on a two-stage strategy, which utilizes a positioning error mechanism model to fit and predict the coupling relationship between the kinematic values of the assemblies and the output positioning error in the pre-compensation stage, and a half-mechanism model to predict the positioning error in the exact compensation stage, which significantly improves the manufacturing accuracy of the aircraft products [21].

This paper introduces the idea of precision control, establishes a simulation model of aircraft assembly process based on precision control, and proposes a visualized assembly process including product model import, resource model import, process information processing, clamping process simulation and assembly path simulation. A method of precision control of aircraft assembly based on parallel configuration is proposed, which realizes the 6-degree-of-freedom alignment and positioning of aircraft components through different mounting arrangements to meet the high-precision assembly requirements of the aircraft. The assembly deviation analysis method based on discrete point set variation extracts the layer, order and constraint information of the vehicle assembly and gives the assumption conditions, constructs the assembly deviation transfer analysis model, describes it in terms of

logical structure and mathematical expression, and gives the variation rules of the characteristic points according to different types of tolerance information. Finally, the effectiveness of the optimization method is verified by experimental results.

2. Assembly process optimization strategy based on precision control

The production accuracy of the existing aircraft assembly is mainly controlled by the production inspection report, and the impact of the assembly process on the assembly accuracy is not fully considered in the assembly process design stage. In order to better realize the assembly accuracy control, it is necessary to use digital simulation means to carry out finite element analysis of assembly accuracy in the process of assembly process design, so as to find out the key characteristics of the assembly accuracy exceeding the tolerance in advance, and thus be able to optimize the assembly process of the aircraft in a targeted manner. This paper introduces the idea of precision control in the process of aircraft assembly process design, and establishes a simulation model of aircraft assembly process based on precision control. A method of precision control of vehicle assembly based on parallel configuration is proposed, which can realize the 6-degree-of-freedom attitude and positioning of the vehicle components through different mounting arrangements to meet the high-precision assembly requirements of the vehicle.

2.1 Simulation model of aircraft assembly process

The visual assembly process simulation based on precision control is shown in Figure 1, which mainly includes five parts: product model import, resource model import, process information processing, clamping process simulation and assembly path simulation [22].

(1) Product model import

According to the supporting parts information in the assembly process information from the three-dimensional digital assembly process (PDM) system into the three-dimensional product model, assembly components to lightweight overall model import, thereby reducing the model size, improve the efficiency of the

assembly process simulation.

(2) Resource model import

According to the supporting resource information in the assembly process information, the 3D resource model is imported from the knowledge base of the aircraft assembly process. According to the actual assembly environment to establish a virtual assembly scene, in order to carry out the clamping process simulation and assembly path simulation.

(3) Processing of process information

Analyze the assembly process information, extract the assembly constraint features and assembly constraint pair information, analyze the assembly operation set used to realize the assembly constraint pair, the required assembly resources such as assembly equipment, fixtures, tools, and assembly parameters, and establish the assembly operation finite element.

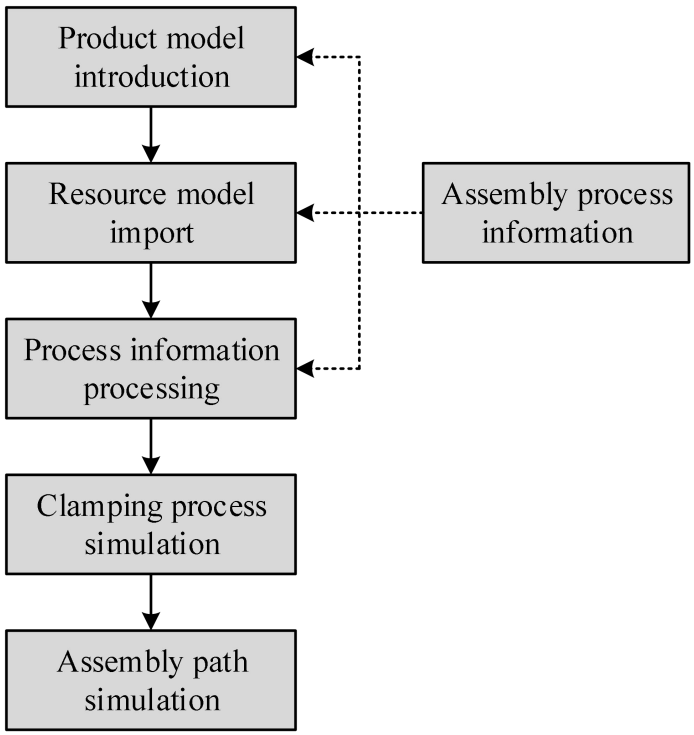

Figure 1 Assembly process simulation based on precision control

(4) Clamping process simulation

Due to the structural characteristics of the aircraft, the assembly process includes a large number of tooling positioning operations, through the clamping simulation can be predicted in advance whether the positioning of the parts of the clamping process is

appropriate, and to put forward suggestions for modification.

(5) Assembly path simulation

The assembly process of the aircraft requires the use of a large number of assembly resources, such as type frame, crane, etc. In order to ensure that the aircraft assembly process does not occur in the assembly path interference, assembly position interference, insufficient accessibility of the installation, etc., it is necessary to carry out the assembly path simulation in advance, in order to avoid rework and repair due to the problem of the assembly path.

2.1.1 Assembly constraint characteristics

An assembly constraint feature is one or more related assembly constraint sets formed after one consecutive assembly between the parts to be assembled and the assembly target during the assembly operation of a vehicle, which describes the assembly constraint relationship between multiple parts, including the constraint feature accessory parts, the reference parts, the assembly constraint set, and the assembly accuracy that the assembly constraints are intended to achieve. Therefore, assembly constraint feature AC_i can be expressed as:

$$AC_i = \{Parts_i, DatumPrt_i, Con_i, Ano_i\} \tag{1}$$

where $Parts_i$ - the set of parts attached to the assembly constraint feature, which can be segments, components, assemblies, or parts.

$DatumPrt_i$ - The datum parts corresponding to the assembly constraint feature.

Con_i - The set of assembly constraints contained in the assembly constraint feature.

Ano_i - The assembly accuracy and assembly requirements to be achieved by the assembly constraint feature.

Assembly constraints include the type of assembly constraint, the parts attached to the assembly constraint, the datum parts, the geometric elements on which the constraint acts, and the assembly accuracy to be achieved by the assembly constraint.

Thus, an assembly constraint Con_i can be represented as:

$$\begin{gathered} Con_i = \{Parts_i, DatumParts_i, Con_{npe}, Geo_i, Ano_i\}, \\ Con_{type} \in \{Con_{joint}, Con_{mate}, Con_{motion}\}, \\ Ano_i \in \{Ano_d, Ano_l, Ano_m, Ano_a, Note, Mark\}. \end{gathered} \tag{2}$$

Where, $Parts_i$ - the accessory parts of the assembly constraint, which can be segments, components, assemblies, or parts.

$DatumPrt_i$ - The reference part of the assembly constraint.

Con_{npe} - the type of constraint.

$Con_{joint}, Con_{mate}, Con_{motion}$ represents the connection constraint, fit constraint and motion constraint of the assembly respectively.

Amo_i - Assembly accuracy and assembly requirements to be achieved by the assembly constraint.

$Ano_d, Ano_l, Ano_m, Ano_a, Note, Mark$ Indicates dimensional accuracy annotations, positional accuracy annotations, kinematic accuracy annotations, contact accuracy annotations, comments, and markings, respectively.

2.1.2 Assembly process simulation

Assembly process consists of a number of assembly processes, assembly process is a workplace, by a worker or a group of workers, the use of a set of assembly equipment to complete that part of the assembly work continuously. An assembly process generally uses only one set of assembly equipment Therefore, assembly process $Process_i$ can be expressed as:

$$Process_i = A_i \bigcup \sum_{j=1}^{n_i} Step_j \bigcup GIPA_i \tag{3}$$

Where, A_i - Attribute information of the assembly process, such as process number, process name, whether it is a critical process or not.

$Step_j$ - One assembly work step contained in the assembly process.

n_i - The total number of assembly steps contained in this assembly process.

$GIPA_i$ - The generalized assembly process model corresponding to the assembly process.

An assembly process consists of multiple assembly steps, which are consecutive assembly tasks taken to complete the installation of one or more assembly objects. In an assembly work step, the assembly objects, assembly tools and assembly methods are unchanged. In order to facilitate process decision making, this paper agrees that an assembly work step completes the assembly of an assembly constraint group. Therefore, the assembly work step $Step_i$ can be denoted as:

$$Step_i = A_i \bigcup \sum_{j=1}^{n_i} OPE_j \bigcup \sum_{k=1}^{m_i} Prt_k \bigcup \sum_{l=1}^{o_i} Tool_l \bigcup Param_i \tag{4}$$

Where: A_i - Attribute information of the assembly work step, such as work step number, operation description, etc.

OPE_i - One assembly operation element that makes up the assembly work step.

n_i - The number of assembly operands contained in the assembly step.

Prt_k - An assembly object of the assembly step.

m_i - The number of supporting parts to be assembled by the assembly step.

$Tool_l$ - The assembly tools used by the assembly step.

o_i - The number of assembly tools used by the assembly step.

$Param_i$ - Assembly parameter information, such as tightening torque.

2.1.3 Assembly information labeling

The association between technical annotation and assembly process can be realized by associating the extension layer and application layer in the assembly process model based on precision control. In order to effectively associate the technical annotation with the assembly process, the paper adopts the assembly process segmentation method based on temporal granularity, which divides, manages and

associates the 3D technical annotation information in accordance with the assembly process granularity and assembly time granularity, and displays it under a specific granularity. The technical framework of the assembly information annotation method based on temporal granularity is shown in Fig. 2, which demonstrates its logical framework relationship, and is realized in the paper by extending the metadata of the assembly model.

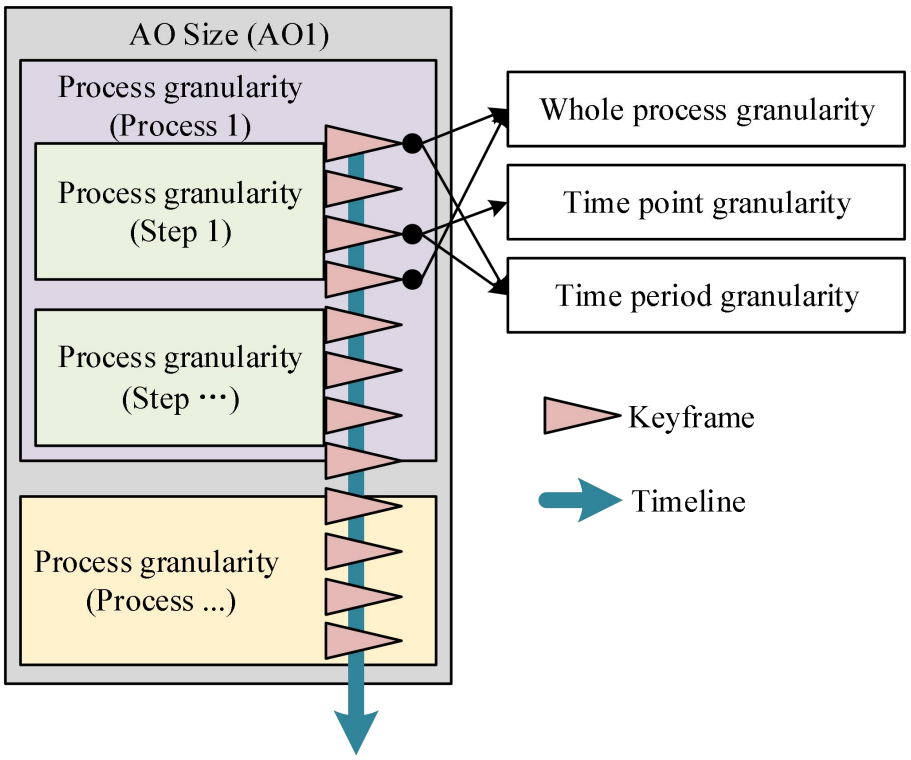

Figure 2 Time sequence granularity segmentation and its annotated framework

The assembly time granularity is categorized into three granularities: full process, time period and point in time. The full process granularity means that the technical annotation is displayed all the time throughout the process, the time period granularity means that the assembly process information annotation only appears for a period of time in the process, and the point in time granularity means that the assembly process information annotation only appears at a specific point in time, where the simulation motion can be paused in order to facilitate the observation of that assembly process information annotation.

2.2 Optimization of assembly accuracy control based on parallel configuration

2.2.1 Positioning and attitude mechanism

In order to realize the 6-degree-of-freedom attitude positioning function of the vehicle wall plate, a 3-UPS parallel mechanism is used to realize the assembly and positioning of the wall plate of a certain type of vehicle [23]. The 3-UPS parallel mechanism is shown in Fig. 3, which mainly consists of a fixed platform $A_1A_2A_3$, a movable platform $B_1B_2B_3$, and three identical struts connecting the movable and fixed platforms. Each strut chain consists of a Hook hinge U , a moving vice P, and a ball hinge vice S , where the outer radius of the fixed platform $A_1A_2A_3$ and the moving platform $B_1B_2B_3$ are R_A and R_B , respectively, and l_i (i = 1, 2, 3) is the distance between the points A_i and B_i .

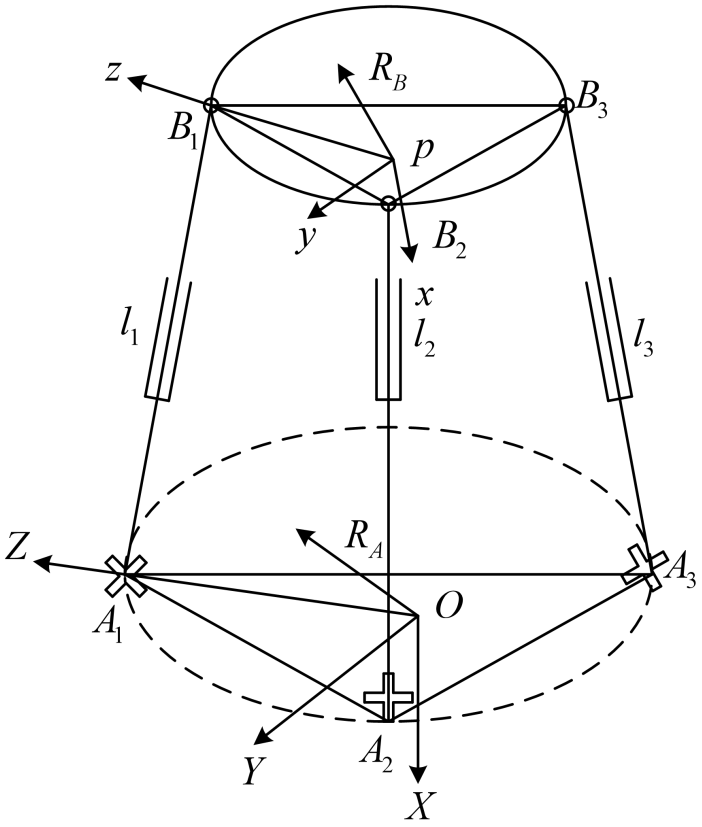

Figure 3 The 3-UPS parallel mechanism

Aiming at the structural characteristics of the parallel mechanism tooling and the

assembly process of the aircraft wall plate, the control system of each drive vice of the parallel mechanism is based on the positioning data generated by offline programming to drive the parallel mechanism to move and carry out the assembly and positioning work of the aircraft wall plate.

2.2.2 Modeling of positioning errors

Clearance errors in the 3-UPS parallel mechanism in the Hook Hinge U and Ball Hinge Sub S can lead to changes in the mechanism's orientation. Manufacturing errors in the hoke hinge shafts and pins can result in an eccentricity distance that can be created after assembly. The Hooke hinge clearance model is shown in Fig. 4, where the eccentricity is considered as a rigid "massless rod", with the rod length represented by vector r_a and the azimuthal angle δ_a.

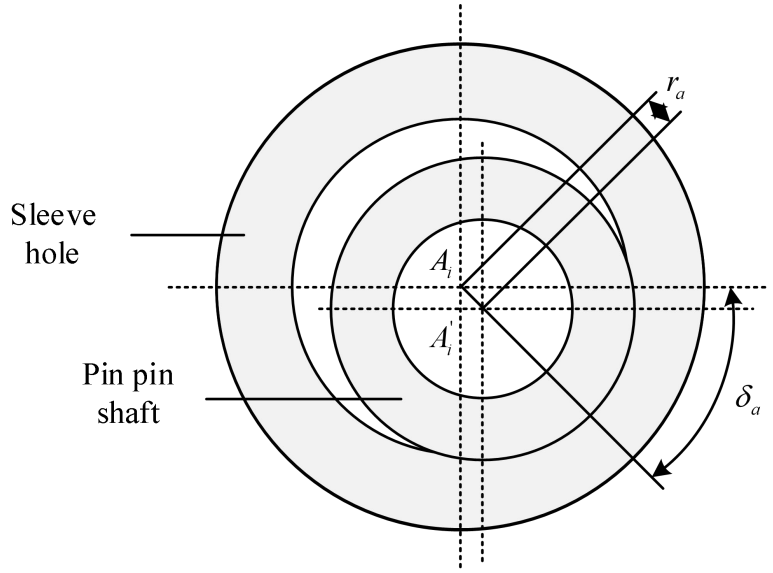

Figure 4 Clearance model of universal joint

In the ball-hinged vice, the ball head of the ball-hinged vice will be offset in the ball fossa due to the gap, and the ball-hinged gap model is shown in Fig. 5. The space vector r_b is used to represent the clearance between the ball-hinged head and the ball fossa, and δ_b is the azimuth angle of the ball-hinged clearance.

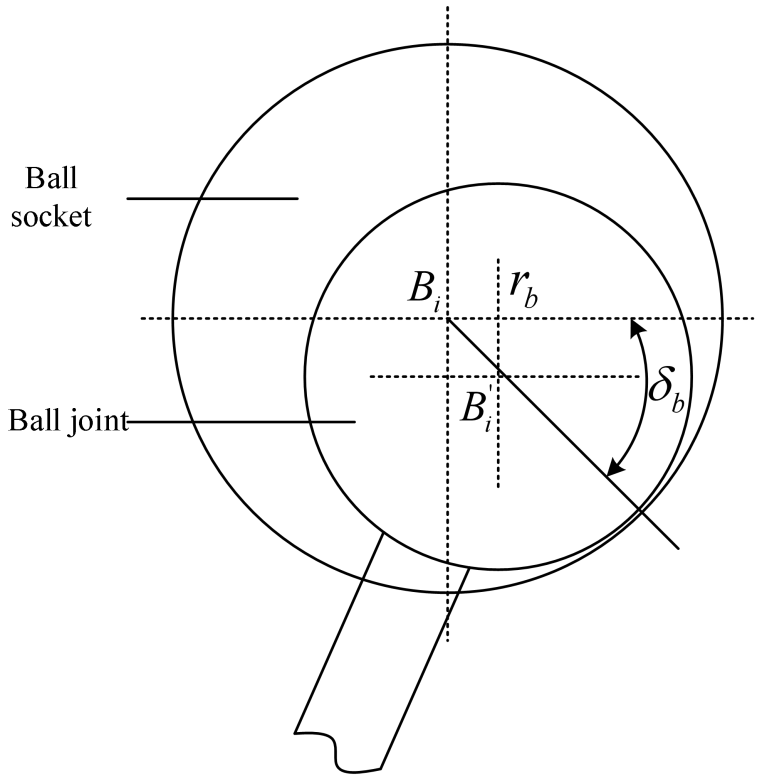

Figure 5 Clearance model of spherical joint

The change of the position of the 3-UPS parallel mechanism is shown in Fig. 6 after considering the gap between the upper and lower hinges of each branch chain. The position of the moving platform changes from the theoretical position B_1, B_2, B_3 to the actual position B_1', B_2', B_3'. Due to the existence of the eccentricity r_a, r_b of each rotating pair and the ball hinge, the effective rod lengths of all the three branch chains of the mechanism change, and the angle with the fixed platform also changes.

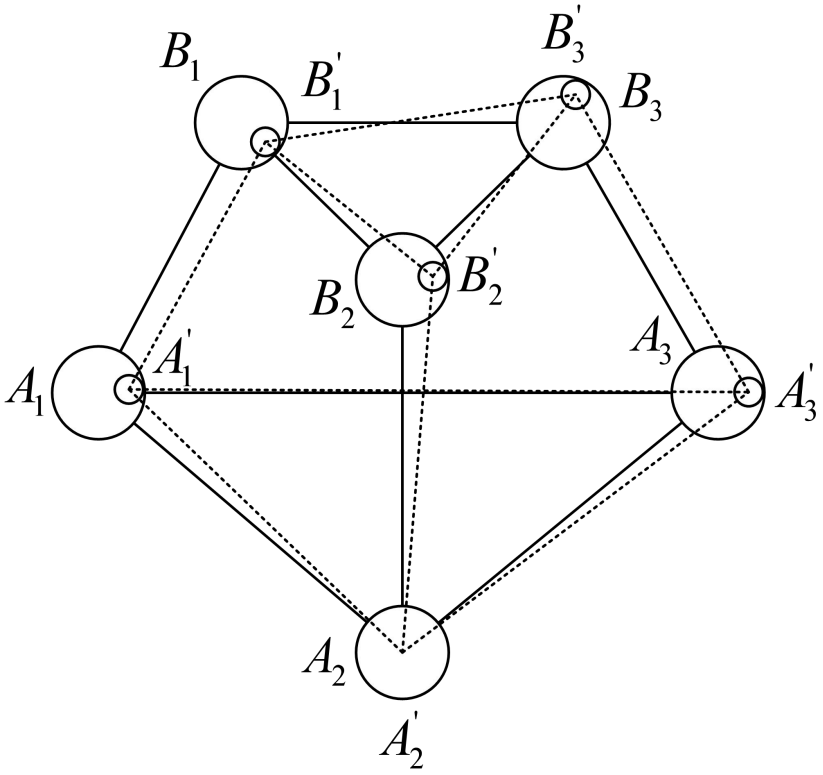

Figure 6 Position and pose model of 3-UPS parallel mechanism considering clearance

When the angle of the first rotating pair of the Hooke hinge is $\psi_i (i = 1,2,3)$ and the angle of the second rotating pair is $0°$, it is shown in Fig. 7. After considering the "massless rod" formed by the error caused by the first rotation of the Hooke's hinge and the ball hinge gap, the effective value of the rod length is $l_{\Lambda_i B_i}$ [24].

The closed-loop vector equation is obtained:

$$l_{A_i B_i} + B_i B_i^{'} = A_i A_i^{'} + l_{A_i' B_i'} (i = 1,2,3) \tag{5}$$

Express it in plural form as:

$$l_{A_i' B_i'} \exp(i\varphi_i^{'}) = l_{A_i B_i} \exp(i\varphi_i) - r_a \exp(-i\delta_{ai}^{'}) + r_b \exp(-i\delta_{bi}^{'}) \tag{6}$$

Separating the imaginary and real parts of Eq. (5) gives:

$$\begin{cases} l_{A_i' B_i'} \cos\varphi_i^{'} = l_{A_i B_i} \cos\varphi_i - r_a \cos\delta_{ai}^{'} + r_b \cos\delta_{bi}^{'} \\ l_{A_i' B_i} \sin\varphi_i' = l_{A_i B_i} \sin\varphi_i + r_a \sin\delta_{ai}' - r_b \sin\delta_{bi}' \end{cases} \tag{7}$$

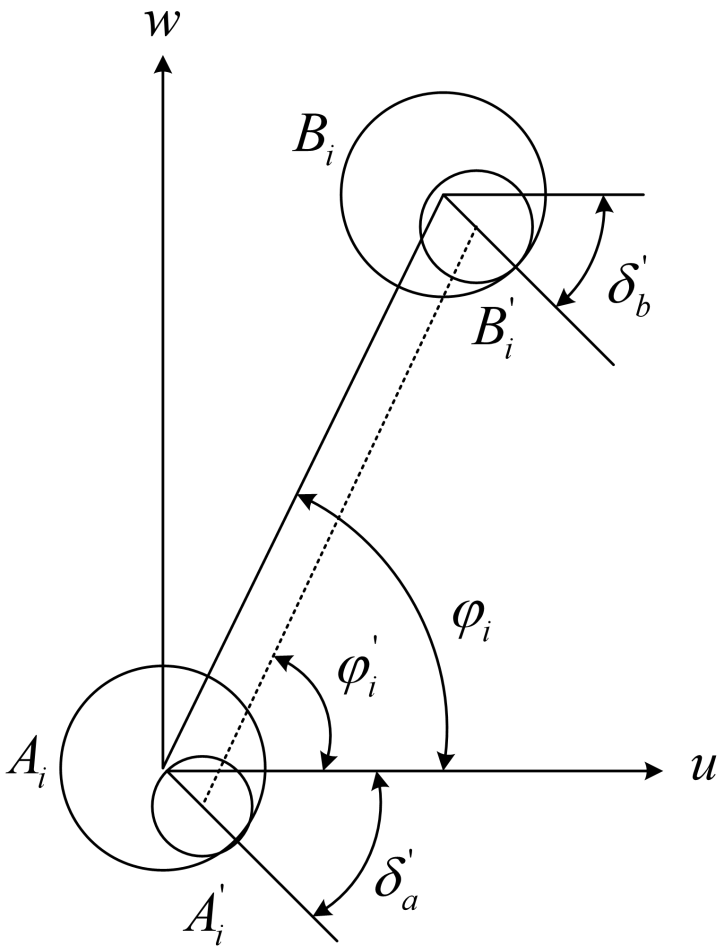

Figure 7 Effective length model on plane uw when $\theta_i = 0°$

The effective rod length model for each strut after taking into account the rotating sub and ball hinge clearance is then obtained by squaring both sides of equations (6) and (7) and using (when x is small) $\sqrt[n]{1+x} \approx 1 + x/n$ [25]:

$$l_{A_i'B_i'} = l_{A_iB_i} + r_b \cos(\varphi_i + \delta_{bi}^{'}) - r_a \cos(\varphi_i + \delta_{ai}^{'}) \tag{8}$$

The mechanism achieves the desired given position when the first rotation sub angle of the Hooke hinge is $\varphi_i (i = 1,2,3)$ and the second rotation sub angle is $\theta_i (i = 1,2,3)$. The final effective rod length of the mechanism at this point is $l_{A_i''B_i''}$.

The closed-loop vector equation is obtained:

$$l_{A_i'B_i'} + B_i'B_i'' = A_i'A_i'' + l_{A_i''B_i''} (i = 1,2,3) \tag{9}$$

Similarly, the effective rod length model of the final mechanism is solved for:

$$l_{A_i''B_i''} = l_{A'iB''i} + r_b\cos(\theta_i + \delta_{bi}'') - r_a\cos(\theta_i + \delta_{ai}'') \tag{10}$$

Substituting Eq. (8) for Eq. (10) yields:

$$l_{A_i''B_i''} = l_{A_iB_i} + \Delta l \tag{11}$$

where Δl represents the length of the "massless bar" produced by the combined action of the gaps in the Hook and Ball hinges:

$$\Delta l = r_b[\cos(\varphi_i + \delta_{bi}') + \cos(\theta_i + \delta_{bi}'')] - r_a[\cos(\varphi_i + \delta_{ai}') + \cos(\theta_i + \delta_{ai}'')] \tag{12}$$

3. Assembly deviation transfer analysis model

3.1 Assembly Information Extraction

The assembly deviation transfer model needs to contain three parts, including assembly hierarchy information, assembly sequence information, and fit constraint information.

3.1.1 Assembly level information

Aircraft products have a large number of parts and complex structure, considering the needs of production process, use and maintenance, the aircraft is divided into different assembly units, and the corresponding key product characteristics of the aircraft are decomposed. The assembly level information of the aircraft product is used to describe the subordination and correlation relationship among the product, subassemblies and parts. Since this paper adopts the variation of feature changes to carry out the assembly deviation analysis, and the feature points are used as the information carrier of deviation transfer, considering the subordination relationship among the parts, feature surfaces and feature points, the assembly deviation transfer analysis model constructed in this paper incorporates them into the assembly level information, which is convenient for analyzing deviation analysis in 3D environment.

3.1.2 Assembly sequence information

Vehicle assembly contains a large number of jigs and fixtures, and the assembly accuracy is required. Different coordination routes actually reflect different assembly

sequences and assembly benchmarks. The assembly sequence indicates both the front and back order of component assembly and determines the characteristics of the fits involved in deviation transfer, i.e., the assembly sequence information describes the front and back order of assembly deviation transfer.

3.1.3 Assembly constraint information

The assembly process is to complete the process of combining and connecting parts according to the design requirements. The assembly process is generally divided into two steps:

First, according to the positioning reference will be assembled accessories positioning in its required spatial position.

Then, using the required connection method to be fitted parts fixed in the assembly body. Positioning errors occur during the positioning process under the action of the fit reference, and deformation errors occur during the clamping and joining process due to the influence of over-constraints and assembly forces.

The fit constraint information is used to describe the assembly process of the assembly body in the space attitude of the constrained state, the constraint relationship exists in the assembly to be assembled sports has been assembled on the mating surface, and in the fit constraints at the formation of the assembly error, the error will be accumulated with the assembly process, and ultimately affect the quality of the assembly.

As the aircraft assembly contains a large number of parts, fixtures and fixtures semantic connectors, etc., there are a large number of fit constraints between them, which are now categorized as follows:

(1) Size and shape constraints within the parts.

(2) Fitting constraints between parts and fixtures.

(3) Fitting constraints between parts. After multiple zero parts are connected to form an assembly, and the subassembly is regarded as a whole, the constraint relationship between components is transformed into the internal constraint of the subassembly.

3.2 Logical structure of assembly deviation transfer

Analyzing the process of assembly deviation transfer in aircraft, we take the refinement and decomposition of fit constraints as a clue to construct an assembly deviation transfer analysis model. The assembly level information is represented by three layers, namely, component layer, feature surface layer and feature point layer, and the hierarchical structure of "top-down, layer-by-layer decomposition" is adopted to complete the decomposition of product functions and structures. The assembly sequence and fit constraints are represented by the assembly constraint diagram.

(1) Assembly constraint graph (ACG)

It represents all the parts in the assembly, their assembly order and the fit relationship and other information. The nodes of the ACG are used to represent the assembly objects it describes, such as components, feature surfaces, and feature points, and the ACG contains directed and undirected edges, where the directed edges indicate the existence of fit constraints between the nodes and the direction of the nodes indicates the assembly order of the nodes, and the undirected edges indicate the existence of dimensional or connectivity relationships between the nodes.

(2) Fit feature pair (AP)

The fit constraint relationship between components is carried by a pair of feature surfaces between parts, and the feature surface carrying the constraint relationship becomes a fit feature pair.

The mapping and inheritance relationships between different levels are described by dotted lines, and the fit constraint relationships are gradually refined through the component level, to the feature surface level, to the feature point level, and are continuously accumulated and transmitted through the discrete point set along with the tolerance information carried.

3.3 Mathematical representation of assembly deviation transfer

Combining the above relevant information in the assembly deviation transfer process, a mathematical representation of the assembly deviation transfer model is given on the basis of the tree model:

$$AVPA = \{P, F, Pnt, M, N\} \tag{13}$$

Where, $AVPA$ - assembly deviation transfer analysis model.

P - Layer of components.

F - feature surface layer.

Pnt - feature point layer.

M - Data mapping between the layers.

N - Constraint mapping between the layers.

(1) $P = \{U^1, E^1\}$ --Parts and components layer

The identification and constraint relationships of the zero components are represented with zero components and workpieces as nodes (workpieces are regarded as special zero components). Where $U^1 = \left\{u_1^1, u_2^1, \ldots, u_{np}^1\right\}$ represents the set of component nodes and np represents the number of nodes in the component layer.

(2) $F = \{U^2, E^2\}$ - Feature face layer

The feature faces are used as nodes to describe the identification and constraint relations of the feature faces. The constraint relationship expresses the fit tolerance information between the feature faces. $U^2 = \{u_1^2, u_2^2, \cdots, u_{nF}^2\} = \{f_{1,1}, f_{1,2}, \cdots, f_{i,j}, \cdots, f_{np,nf}\}$ represents the feature face.

(3) $Pnt = \{U^3, E^3\}$ - Feature point layer

With feature points as nodes, it records the aggregate relationship of feature face to feature point transformation.

(4) $M = \{m^{ij} \mid m^{ij} = (u^i, u^j), u^i \in U^i, u^j \in U^j, i, j \in [1,3]\}$ - Data mapping between levels.

(5) $N = \{n^{ij} \mid n^{ij} = (e^i, e^j), e^i \in E^i, e^j \in E^j, i, j \in [1,2]\}$ - Constraint mapping between levels.

Since the vehicle components are all rigid bodies, their deformation is not considered for the time being in the assembly deviation analysis, and their assembly accuracy can be recognized as the result of the transfer and accumulation of

manufacturing and positioning deviations.

4. Numerical examples and experimental analysis

In order to verify the effectiveness of the method proposed in this paper, the positioning accuracy of the 3-UPS positioning and attitude adjustment mechanism under the coupling of elastic deformation error of the parallel mechanism and elastic deformation error of the components is firstly calculated numerically, and the assembly and attitude trajectory with optimal integrated error degree is calculated in conjunction with the vehicle assembly process based on precision control. Then, an experimental platform is built to experimentally verify the optimization and compensation of the method in this paper.

4.1 Example simulation

In this paper, the finite element analysis process is carried out for the designed test pieces so that the results can be compared with the actual test results to verify the correctness of this paper's method.

In order to reflect as much as possible the actual situation when the components are docked with unidirectional compression holes, the experimental parts are designed by applying St. Venant's principle and selecting a small section of the annular region at the docking place of the head and the forward fuselage components of a commercial aircraft.

The docking structure of the vehicle components is shown in Fig. 8, and the following principles are used to design the experimental conditions based on the typical structure of the docking:

(1) The main research part of this paper is the strip plate area between the long truss joints, so it is necessary to intercept a section of the circumferential length model containing at least 2 long trusses from the digital model to meet the experimental demand for making holes in a typical strip plate, and at the same time try to maintain the symmetry of the model, so as to make it well-balanced and stable, and it is easy to impose constraints.

(2) The bottom plates of the fuselage frame and the nose frame in the actual

working condition have all been connected with rivets on the skin fitting surface. Since the frame is structurally stable and rigid, the frame can be regarded as a solidly supported part. All the outermost side of the bottom plate is intercepted as the boundary, and the skin and long truss boundaries of the intercepted and frame connections are regarded as solidly supported.

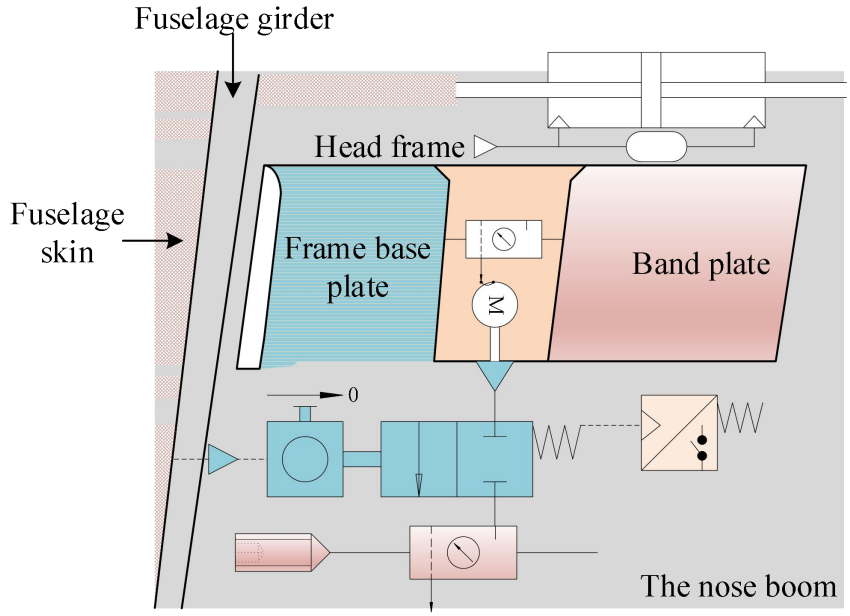

Figure 8 The docking structure of the aircraft components

(3) Since the long truss joint is not yet assembled and connected with the strip plate and the skin, it will not affect the gap between the strip plate and the skin fitting surface of the main study, and the test piece is chosen to ignore the long truss joint.

(4) According to the actual structural dimensions and St. Venant's principle, the dimensions of the skin and strip plate in the length direction are intercepted to be 700mm.

(5) A set of fixture is designed to fix the test piece. Since the aircraft parts are thin-walled parts, the fixture is required to ensure the stiffness of the experimental parts. Also ensure that the fixture and equipment is easy to disassemble, easy to operate. Design as much as possible to use outsourcing parts, such as the possible use of C-clamps, to reduce processing costs and cycle time.

Limitations of space, this paper in the band plate on the column of holes in every 3 holes on a pre-assembled fastening bolts on the test piece as an example to illustrate

the finite element analysis process.

In the analysis, the test pre-tensioned spring clamp is replaced by a bolt, and the pre-tensioning force is replaced by applying a bolt load. The holes for the finite element analysis are shown in Fig. 9, where the preloaded nails are installed at A, B, C and D. It is proposed to analyze the compression force, and the effect of such pre-assembly on the skin gap for areas 2 and 4 in the figure.

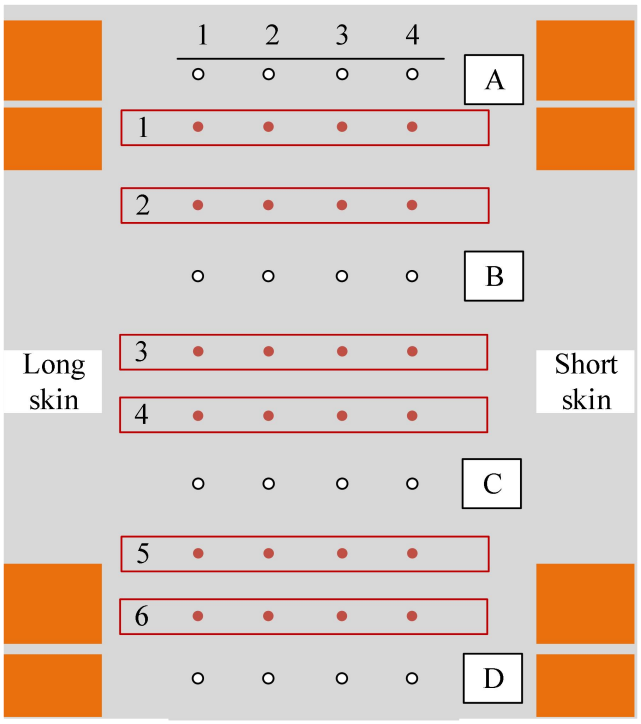

Figure 9 Hole location of finite element analysis

Since the test piece models for this analysis are all regular cubes, the cell mesh type of eight-node hexahedral linear reduced integration cell C3D8R is used for the skin, strip plate, and pre-assembled bolts. Using the simple master-slave contact pair algorithm, the mesh density of the slave surface should be denser than the master surface, in order to obtain a better contact simulation.

The basic assumptions of the simulation process are as follows:

(1) The geometric deformation of the part conforms to the small deformation theory.

(2) The part is isotropic linear elastic material.

(3) The tolerance of the fitting surface is negligible.

The materials used in the skin and belt plate of this test part are all purchased

2024 aluminum alloy materials, with a modulus of elasticity of 70 MPa and a Poisson's ratio of 0.35. The modulus of elasticity of the pre-assembled bolt is 250 MPa and a Poisson's ratio of 0.25.

The contact is defined as setting the initial condition of the contact as not adjusting the position of the master and slave surfaces, and selecting the small slip and point opposite discrete mode. The preload force applied by the preload bolts is 100 N. The boundary conditions are defined as follows: only the split surfaces on the left and right sides of the skin restrict the degrees of freedom of the end surfaces U1, U2, and U3 (which are solidly supported), and the rest are not constrained.

The load conditions are, unidirectional compression force, gradually increasing from 200N to 1200N (increment of 100N), and the axial cutting force of the hole-making spindle is 100 N. Firstly, the drilling force is applied to the strip plate, and the unidirectional compression force is applied to the skin to analyze the trend of the gap value of the contact surface of the skin and the strip plate with the compression force.

According to the actual working conditions, the maximum value of clearance should exist for drilling these 24 holes.

4.2 Analysis of experimental results

4.2.1 Optimization of cooperative motion trajectories of the attitude mechanism

Experimental verification of cooperative motion trajectory optimization is carried out on the constructed 3-UPS parallel mechanism, and the trajectory with the optimal integrated error degree is imported into the control system to drive the cooperative motion of positioners 1 and 2 of the parallel mechanism in the course of attitude adjustment. A total of 24 positioning attitude measurement points are set up on the lower and side wall panels, and when the system moves through each discrete step, the laser tracker measures the actual positions of the 24 points, respectively, and records them. In order to verify the effectiveness of this paper based on the 3-UPS parallel configuration positioning attitude method, a comparison experiment is designed in the experimental process. The comparison experiment also divides the

precise motion process into five steps, but fixes the motion of the redundant axes under each step, i.e., does not consider the multi-resolution characteristic of the tuning range caused by redundancy. In this case, there exists a uniquely determined trajectory during the collaborative attitude-tuning motion of the lower and sidewall panels, and the real-time position data of 24 measurement points are universally collected.

The evaluation error degree and the integrated error degree under the two experimental methods are shown in Fig. 10. From the experimental results, it can be seen that adopting the attitude adjustment trajectory with the optimal integrated error degree can effectively reduce the positioning error, which verifies the correctness and feasibility of the method in this paper. Finally, through the experiment to verify the tuning task of the tuning mechanism containing redundant degrees of freedom, the results show that the optimal tuning trajectory with the integrated error degree has a comprehensive error degree of 0.134mm, which meets the demand for the tuning accuracy of the aircraft assembly.

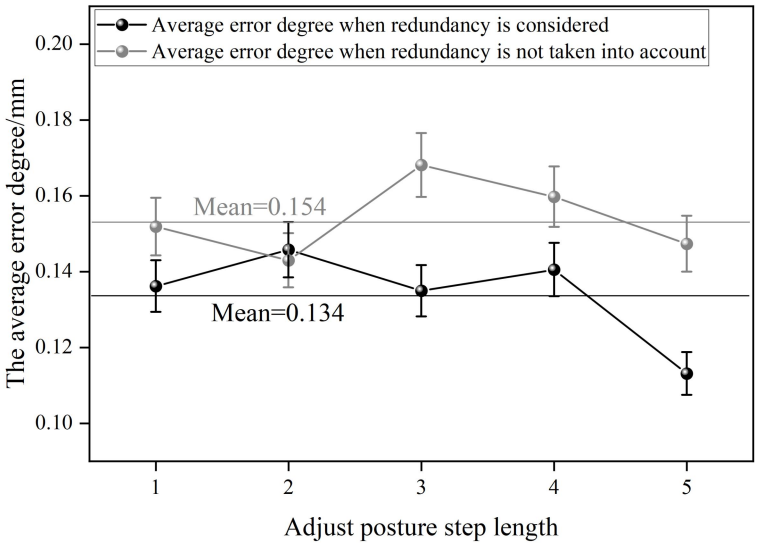

Figure 10 Average error degree during attitude adjustment

4.2.2 Optimization of force-position synergistic control in the attitude adjustment process

The method in this paper is used to calibrate and compensate the geometric errors of the left and right side sill parallel positioners and the top sill parallel positioner in the fuselage attitude mechanism in the aircraft. The 100 coordinated positional points in the collaborative motion space of the attitude mechanism are

selected, and the left and right side sill and top sill parallel positioners are driven to reach the set coordinated positional points. The absolute positioning accuracy and relative positioning accuracy of each parallel positioner are recorded by laser tracker respectively.

In the process of utilizing the center fuselage attitude adjustment mechanism based on the parallel configuration, the force-position control method is adopted to control the attitude adjustment internal force. In order to guarantee the effectiveness of the force-position control method, it is first necessary to simulate and analyze the force-position system control method in the simulation system.

The simulation platform in Section 4.1 is used to calculate the mass of the fuselage left side ledge as 620kg through CAD software, and the initial coordinates of the ball-hinge center point under the dynamic platform are B_1 (-1250,0,-500), B_2 (1250,0,-500), (1250,0,500), B_3 (-1250,0,500), B_4 (-1250,0,500), respectively. The initial position of the simulation is (-10,100,40, $5°$,- $5°$, $5°$), the target position is the fuselage sill mounted in place position (0,400,0,0,0,0), and the simulation time is set to 200s.

The results of absolute position error and absolute attitude error before and after calibration are shown in Table 1, which shows that during the assembly process of the vehicle, the absolute position and absolute attitude errors of the left side siding are 1.051mm and 0.813º before calibration, and 0.234mm and 0.322° after calibration, both of which are maximum.

Table 1 Absolute position error and attitude error before and after calibration

Fuselage component		Absolute position error mean/mm	Absolute attitude error mean/º
Left side wall panel localizer	Pre-calibration	1.051	0.813
	After-calibration	0.234	0.322
Right side wall panel localizer	Pre-calibration	0.938	0.735
	After-calibration	0.245	0.289
Top side wall panel localizer	Pre-calibration	0.785	0.551
	After-calibration	0.197	0.133

Position control and force/bit control methods are used for the left side ledge adjustment process, respectively, and the simulation results of the position error are shown in Figure 11. It can be seen that the minimum value of the left wall plate

positioning error (bit 1~bit 4) is 0.079 mm and the maximum value is 0.115 mm when the posturing mechanism carries out position control, and it increases with the increase of posturing displacement, which is due to the increase of the y-direction cantilever length of the parallel mechanism supporting chain in the process of approaching to the target posturing, and the movement error caused by the gravity and other roles of the wall plate increases. The minimum value of the wall plate positioning error (force/position 1~force/position 4) is 0.049mm, and the maximum value is 0.065mm, and the range of the positioning error during the whole posturing process is small, which meets the requirement of posturing positioning error $\leqslant \pm$ 0.1mm. Simulation results show that the use of force-position synergistic control method for the attitude adjustment mechanism improves the overall attitude positioning accuracy by about 35%.

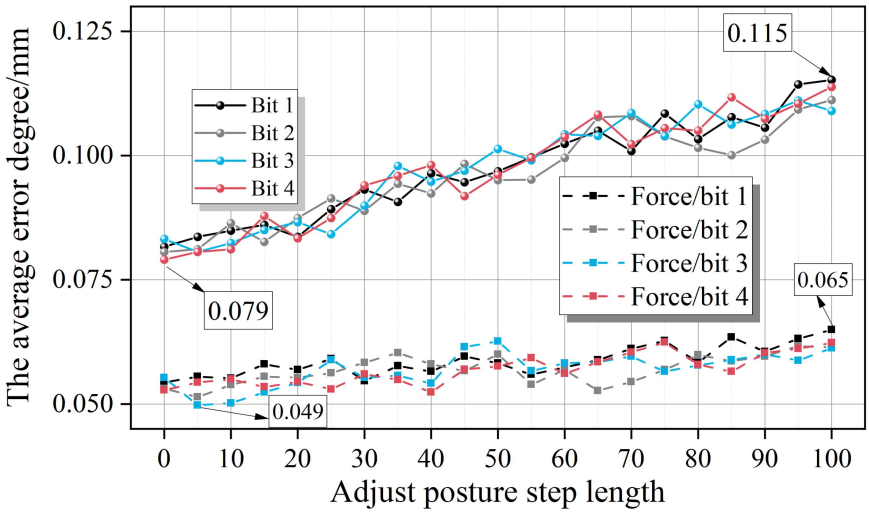

Figure 11 Position error simulation results

The simulation results of the internal force of the left wall plate of the vehicle are shown in Fig. 12. The minimum value of the measured value of the force sensor at the ball hinge of the attitude mechanism (removing the gravity of the wall plate, bit 1~bit 4) when the attitude mechanism carries out the position control is 57.73 N, and the maximum value is 97.95 N. The force sensor changes from a large value to a small value at the beginning of the attitude and rises after that, and there is an accelerating process of the attitude mechanism from static to motion. After the motion is smooth, the force measurement value increases as the error of the y-direction motion of the

parallel mechanism support chain becomes larger. The minimum value of the measured value of the force sensor (force/position 1~force/position 4) is 8.41N, and the maximum value is 18.18N, and the fluctuation range of the measured value of the force sensor during the whole posturing process is small. The simulation results show that the overall internal force of the attitude mechanism can be reduced by about 75% by using the force-position cooperative control method.

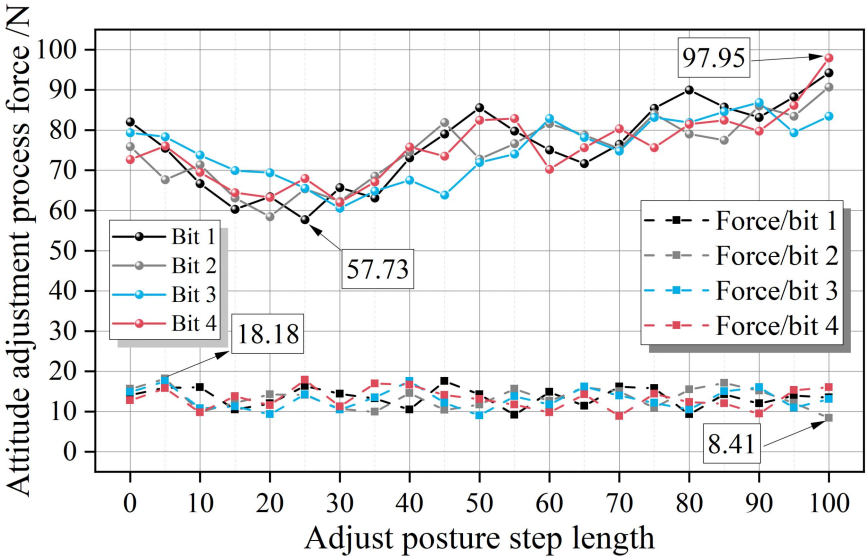

Figure 12 Internal force simulation results of posture adjustment

The attitude adjustment method based on force-position cooperative control proposed in this paper is applied to the fuselage assembly in a large aircraft. Through field experiments, the measured values of the force sensors installed at the ball and socket of the CNC positioner under the two methods of position control and force-position synergistic control are collected as shown in Fig. 13 (one of the force sensors is taken as an example), and the maximum values of the feedback from the force sensors of the two methods are -135N and -28N, respectively (the minus sign indicates the direction of the force action). After the completion of the assembly, through the detection of the positional data of the characteristic points of the middle fuselage, the fuselage assembly accuracy using the force-position system control method is 0.08mm, which meets the requirements of the positioning error $\leqslant \pm$ 0.1mm in the assembly process of the aircraft. The experimental results show that the use of force-position system control method can effectively reduce the internal force of attitude adjustment, ensure the positioning accuracy of attitude adjustment, ensure

the reliability of the component attitude adjustment task, and avoid the damage of the component caused by the excessive internal force of attitude adjustment.

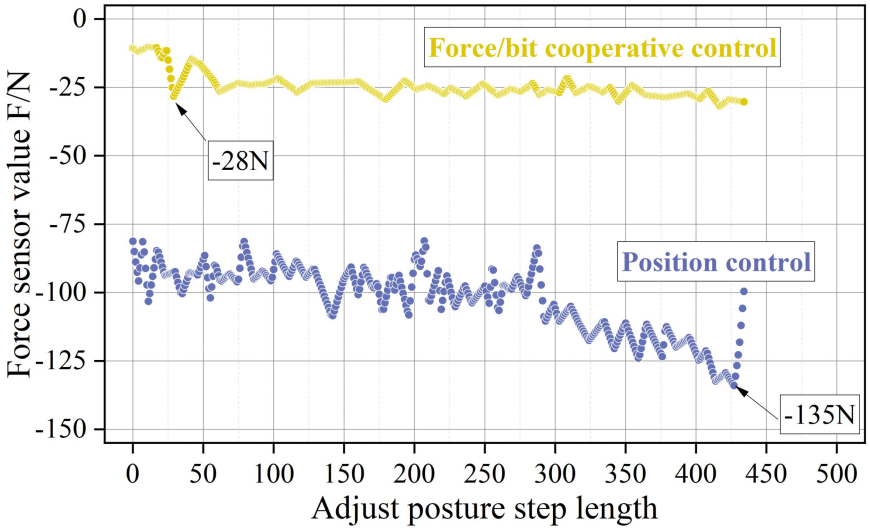

Figure 13 Measured values of the force sensor of the CNC positioner

4.2.3 Optimization of assembly accuracy compensation

The establishment of the 3-UPS error model in this paper synthesizes the three factors of the clearance of the three motion subsets, such as the rotation subset, the moving subset, and the ball-hinge subset, of each pivot chain. The initial structural parameters of the mechanism are now given, and the variation interval of the error gap of each motion vice is shown in Table 2. The maximum azimuth error of assembly accuracy is set to be ±0.2° interval to meet the accuracy requirements of vehicle assembly.

Table 2 Initial structure parameters and error variation interval of 3-UPS mechanism

Factor	Geometric quantity	Dimension parameter
Moving platform radius /mm	r	30
Set the platform radius /mm	R	50
Lower chain design rod length /mm	l_{i1}	72
Upper chain design rod length /mm	l_{i2}	55
Drive rod length /mm	l_i	115.2
Upper and lower chain repeat rod length /mm	H_i	15.6
Rotating pair clearance /mm	r_a	[0.14, 0.18]
Ball joint clearance /mm	r_b	[0.16, 0.20]
Moving secondary clearance /mm	r_c	[0.08, 0.12]
Azimuth/ (°)	θ_i	80
Azimuth error/ (°)	$\Delta\theta_i$	[-0.2, 0.2]
First error Angle/ (°)	δ_a	[0, 360]
Second error Angle/ (°)	ε	[-0.2, 0.2]
Error Angle of ball hinge pair / (°)	δ_b	[0, 360]
Error Angle of moving pair/ (°)	δ_c	[-0.2, 0.2]

Define the nominal trajectory of the 3-UPS parallel mechanism moving platform in the vehicle assembly workspace as (units, mm):

$$\begin{cases} x(t) = 10\sin(\pi t) \\ y(t) = 10\cos(\pi t) \\ z(t) = 120 + \sin(\pi t) \\ t = 0 \sim 2s \end{cases} \tag{14}$$

where $x(t)$ and $y(t)$ denote the nominal attitude of the moving platform and $z(t)$ denotes the nominal position of the moving platform.

According to the given ideal attitude of the moving platform, i.e., the nominal trajectory and the nominal size parameter of the mechanism, as well as the kinematic inverse solution model, the nominal driving function of the driving rod is calculated, and inputted into the actual kinematic orthogonal solution model of the 3-UPS parallel mechanism which contains the kinematic subgap, the actual attitude of the moving platform of the mechanism before the compensation is calculated, and the comparison is made with the structure after the compensation.

The nominal position of the 3-UPS parallel mechanism at the moment of t=0.1s is taken for the optimization of the compensation amount of the driving rod length, and the multi-objective optimization model of the 3-UPS parallel mechanism is established:

Objective function:

$$\min \begin{cases} \left|\Delta\alpha\right| = f_1(\Delta l_1, \Delta l_2, \Delta l_3, \varepsilon, r_a, r_b, r_c, \delta_a, \delta_b, \delta_c) \\ \left|\Delta\beta\right| = f_2(\Delta l_1, \Delta l_2, \Delta l_3, \varepsilon, r_a, r_b, r_c, \delta_a, \delta_b, \delta_c) \\ \left|\Delta z\right| = f_3(\Delta l_1, \Delta l_2, \Delta l_3, \varepsilon, r_a, r_b, r_c, \delta_a, \delta_b, \delta_c) \end{cases} \tag{15}$$

Constraint 1:

$$s.t. \ -0.2 \le \Delta l_1, \Delta l_2, \Delta l_3 \le 0.2 \tag{16}$$

Constraint 2:

$$s.t.\begin{cases} 0.14 \le r_a \le 0.18 \\ 0.16 \le r_b \le 0.20 \\ 0.08 \le r_c \le 0.12 \\ 0^\circ \le \delta_a, \delta_b \le 360^\circ \\ -0.5^\circ \le \delta_c, \varepsilon \le 0.5^\circ \end{cases} \tag{17}$$

The running parameters, population size 500, number of running generations 500, crossover probability 0.9, and population variance probability 0.1. Each under positional attitude of the 3-UPS parallel mechanism corresponds to a set of Pareto solution set, and each set of drive rod compensation corresponds to a solution in that solution set. The Pareto solution set of the 3-UPS parallel mechanism positioning error under the positioning attitude obtained by the NSGA-II algorithm is shown in Fig. 14, and the three axes correspond to the three objective function values. The circled part of the figure indicates the combined optimal point selected by applying the fuzzy set theory for the 3-UPS parallel mechanism at t = 0.1 s positioning attitude.

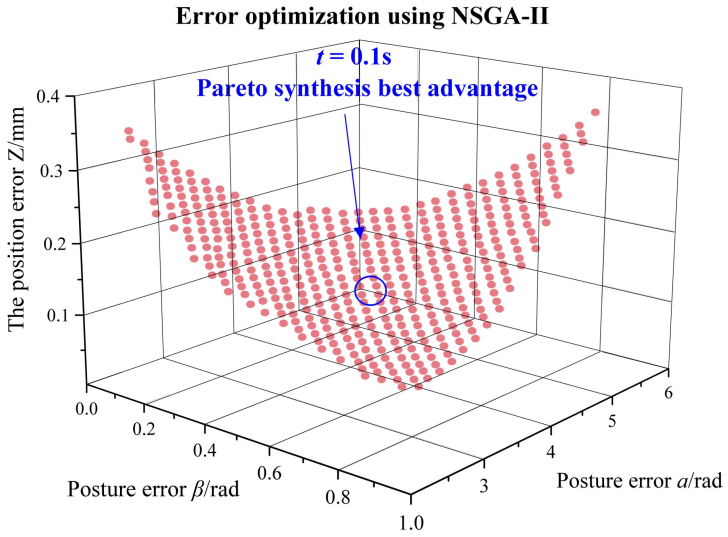

Figure 14 Pareto set of pose error of 3-UPS parallel mechanism and its optimum advantage

Similarly, the optimal drive rod compensation of the 3-UPS parallel mechanism in each nominal position in one cycle (T=2s) can be solved. The 100 optimized drive rod compensation quantities in one cycle are taken uniformly, and the optimized results of the drive rod compensation quantities at each moment of the solution are added to the nominal drive rod lengths at the corresponding moments as new inputs, so as to obtain the trajectories of the reference point of the moving platform after the optimized compensation of the 3-UPS mechanism with the hinge gap, and compare

them with the nominal trajectories as well as the trajectories before the uncompensated trajectories. In order to visualize the results, the spatial distributions of the errors of the moving platform reference point in the degree-of-freedom and non-degree-of-freedom directions before and after compensation are given, and the statistical analysis of the corresponding error components are calculated respectively.

The comparison results of the component errors in the direction of degrees of freedom before and after compensation are shown in Table 3, and the comparison results of the component errors in the direction of non-degrees of freedom before and after compensation are shown in Table 4. After optimizing the compensation using the method in this paper, the maximum angular error of the moving platform around the X-axis and Y-axis is 5.940×10^{-4} rad respectively, which improves the assembly accuracy by two orders of magnitude compared with the 1.18×10^{-2} rad before compensation. The maximum movement error along the three directions of X-axis, Y-axis and Z-axis is 0.037mm, which is one order of magnitude higher compared with 0.371mm before compensation.

Table 3 Comparison of directional component error of DOF before and after compensation

Error	Absolute maximum (Compensation)		Absolute mean (Compensation)		Standard deviation(Compensation)	
	Before	After	Before	After	Before	After
$\Delta\alpha$ /rad	1.18×10^{-2}	5.94×10^{-4}	9.28×10^{-3}	4.21×10^{-4}	1.41×10^{-3}	1.02×10^{-4}
$\Delta\beta$ /rad	3.31×10^{-3}	8.51×10^{-5}	1.95×10^{-3}	5.03×10^{-5}	9.87×10^{-4}	5.55×10^{-5}
ΔZ /mm	0.371	0.037	0.204	0.019	0.114	0.019

Table 4 Comparison of non-DOF directional component errors before and after compensation

Error	Absolute maximum (Compensation)		Absolute mean (Compensation)		Standard deviation (Compensation)	
	Before	After	Before	After	Before	After
ΔX /mm	0.115	0.016	0.061	0.007	0.061	0.007
ΔY /mm	0.167	0.018	0.098	0.009	0.112	0.013

5. Conclusion

In this paper, a flexible positioning mechanism for aircraft assembly based on 3-UPS parallel configuration is designed and the effective rod length model is established with the application background of aircraft fuselage wall plate parts positioning. On the basis of the theoretical study, validation and application studies are carried out on a variety of reconfigurable attitude-tuning equipment, and it is

found that the attitude-tuning and positioning accuracy, as well as the attitude-tuning internal force of the method have been significantly improved. Before the compensation, the maximum angle error of the moving platform around X-axis and Y-axis is 1.18×10^{-2} rad, and the maximum movement error along X-axis, Y-axis, and Z-axis is 0.371mm, and after the optimization of the compensation using the method in this paper, the maximum angle error and maximum movement error of the vehicle assembly are 5.940×10^{-4} rad and 0.037mm, respectively, and the assembly accuracy is significantly improved. At the same time, it also provides new ideas and methods for the development of flexible tooling for aircraft assembly.

References

[1] Guo, F., Wang, Z., Kang, Y., Li, X., Chang, Z., & Wang, B. (2018). Positioning method and assembly precision for aircraft wing skin. Proceedings of the Institution of Mechanical Engineers, Part B: Journal of Engineering Manufacture, 232(2), 317-327.

[2] Fan, W., Zheng, L., Ji, W., Xu, X., Lu, Y., & Wang, L. (2021). A machining accuracy informed adaptive positioning method for finish machining of assembly interfaces of large-scale aircraft components. Robotics and Computer-Integrated Manufacturing, 67, 102021.

[3] Miah, M. H., Zhang, J., & Singh Chand, D. (2022). Knowledge creation and application of optimal tolerance distribution method for aircraft product assembly. Aircraft Engineering and Aerospace Technology, 94(3), 431-436.

[4] Deng, Z., Huang, X., Li, S., & Xing, H. (2019). On-line calibration and uncertainties evaluation of spherical joint positions on large aircraft component for zero-clearance posture alignment. Robotics and computer-integrated manufacturing, 56, 38-54.

[5] Fan, W., Zheng, L., Ji, W., Xu, X., Wang, L., Lu, Y., & Zhao, X. (2020). Function block-based closed-loop adaptive machining for assembly interfaces of large-scale aircraft components. Robotics and Computer-Integrated Manufacturing, 66, 101994.

[6] Mei, B., & Zhu, W. (2021). Accurate positioning of a drilling and riveting cell for

aircraft assembly. Robotics and Computer-Integrated Manufacturing, 69, 102112.

[7] Deng, Z., Li, S., & Huang, X. (2018). Uncertainties evaluation of coordinate transformation parameters in the large-scale measurement for aircraft assembly. Sensor Review, 38(4), 542-550.

[8] Li, S., Huang, Z., Zeng, Q., & Huang, X. (2022). Study of a transferring system for measurements in aircraft assembly. Journal of Intelligent Manufacturing and Special Equipment, 3(1), 31-47.

[9] Zhao, D., Suo, Y., Liu, X., Zhang, D., & Kou, Y. (2024, May). Tolerance Simulation and Optimization Technology for Aircraft Assembly Based on Key Characteristics. In 2024 IEEE 6th Advanced Information Management, Communicates, Electronic and Automation Control Conference (IMCEC) (Vol. 6, pp. 552-556). IEEE.

[10] Zhang, Q., Zheng, S., Yu, C., Wang, Q., & Ke, Y. (2022). Digital thread-based modeling of digital twin framework for the aircraft assembly system. Journal of Manufacturing Systems, 65, 406-420.

[11] Liu, X., An, L., Wang, Z., Tan, C., Wang, X., & Yu, S. (2019). Assembly Variation Analysis of Aircraft Panels under Part‐to‐part Locating Scheme. International Journal of Aerospace Engineering, 2019(1), 9563596.

[12] Cheng, L., Wang, Q., Li, J., & Ke, Y. (2018). Propagation analysis of variation for fuselage structures in multi-station aircraft assembly. Assembly Automation, 38(1), 67-76.

[13] Zhang, L., Wang, H., Li, S., & Lin, Z. (2017). Variation propagation modeling and pattern mapping method for aircraft assembly structure considering residual stress from manufacturing process. Proceedings of the Institution of Mechanical Engineers, Part B: Journal of Engineering Manufacture, 231(3), 437-453.

[14] Jing, T., Tian, X., Liu, X., Hu, H., Zhang, M., & Li, B. (2020). A multiple alternative processes-based cost-tolerance optimal model for aircraft assembly. The International Journal of Advanced Manufacturing Technology, 107, 667-677.

[15] Duan, G., Shen, Z., & Liu, R. (2019). An MBD based framework for relative position accuracy measurement in digital assembly of large-scale component.

Assembly Automation, 39(4), 685-695.

[16] Yuan, L. I., Zhang, L., & Yanzhong, W. A. N. G. (2017). An optimal method of posture adjustment in aircraft fuselage joining assembly with engineering constraints. Chinese Journal of Aeronautics, 30(6), 2016-2023.

[17] Guo, F., Liu, J., Zou, F., & Wang, Z. (2020). Aircraft assembly quality control with feedback actions and assembly station flowing fluctuation analysis. IEEE Access, 8, 190118-190135.

[18] Wang, Q., Dou, Y., Li, J., Ke, Y., Keogh, P., & Maropoulos, P. G. (2017). An assembly gap control method based on posture alignment of wing panels in aircraft assembly. Assembly Automation, 37(4), 422-433.

[19] Guo, F., Zou, F., Liu, J. H., Xiao, Q., & Wang, Z. (2019). Assembly error propagation modeling and coordination error chain construction for aircraft. Assembly Automation, 39(2), 308-322.

[20] Yu, L., Zhang, Y., Bi, Q., & Wang, Y. (2017). Research on surface normal measurement and adjustment in aircraft assembly. Precision Engineering, 50, 482-493.

[21] Guo, F., Liu, J., Wang, Z., Zou, F., & Zhao, X. (2020). Positioning error guarantee method with two-stage compensation strategy for aircraft flexible assembly tooling. Journal of Manufacturing Systems, 55, 285-301.

[22] Cheng Yan,Xu Yuan heng,Huang Xue liang & Wang Lei. (2020). Accuracy Control of Big-scale Space 3D Measurement System in Aircraft Digital Assembly. IOP Conference Series: Materials Science and Engineering012030-012030.

[23] Xing Shiyu,Wang Zhe,Hou Jun,Fan Junfeng,Jing Fengshui & Tan Min. (2022). Component calibration and configuration planning in assembly automation with a parallel manipulator. Robotics and Computer-Integrated Manufacturing.

[24] Soheil Zarkandi. (2020). Kinematic analysis and optimal design of a novel 3-P R R spherical parallel manipulator. Proceedings of the Institution of Mechanical Engineers Part C Journal of Mechanical Engineering Science(4),095440622093880.

[25] Yuan Rui Zhang,Shigenobu Nagase,Jiang Zhu,Tomohisa Tanaka & Yoshio Saito. (2014). Positioning Calibration of a Parallel Mechanism Worktable with 6-DOF. Key Engineering Materials(625-625),392-397.